

Robust Auto-landing Control of an agile Regional Jet Using Fuzzy Q-learning

Mohsen Zahmatkesh^a, Seyyed Ali Emami^a, Afshin Banazadeh^{a,*}, Paolo Castaldi^b

^a*Department of Aerospace Engineering, Sharif University of Technology, Tehran, Iran*

^b*Department of Electrical, Electronic and Information Engineering "Guglielmo Marconi", University of Bologna, Via Dell'Universit'a 50, Cesena, Italy*

Abstract

A robust auto-landing problem of a Truss-braced Wing (TBW) regional jet aircraft with poor stability characteristics is presented in this study employing a Fuzzy Reinforcement Learning scheme. Reinforcement Learning (RL) has seen a recent surge in practical uses in control systems. In contrast to many studies implementing Deep Learning in RL algorithms to generate continuous actions, the methodology of this study is straightforward and avoids complex neural network architectures by applying Fuzzy rules. An innovative, agile civil aircraft is selected not only to meet future aviation community expectations but also to demonstrate the robustness of the suggested method. In order to create a multi-objective RL environment, a Six-degree-of-freedom (6-DoF) simulation is first developed. By transforming the auto-landing problem of the aircraft into a Markov Decision Process (MDP) formulation, the problem is solved by designing a low-level Fuzzy Q-learning (FQL) controller. More specifically, the well-known Q-learning method, which is a discrete RL algorithm, is supplemented by Fuzzy rules to provide continuous actions with no need to complex learning structures. The performance of the proposed system is then evaluated by extensive flight simulations in different flight conditions considering severe wind gusts, measurement noises, actuator faults, and model uncertainties. Besides, the controller effectiveness would be compared with existing competing techniques such as Dynamic Inversion (DI) and Q-learning. The simulation results indicate the superior performance of the proposed control system as a reliable and robust control method to be employed in real applications.

Keywords: Fuzzy Q-learning, Q-learning, Reinforcement Learning, Auto-landing

1. Introduction

Recently, the aviation industry has faced a number of challenges, including increased emissions and congested airspace. As a result, the future world requirements will be characterized as safety and efficiency. In the efficiency segment, reducing emissions by using less fuel and making economical flights alongside faster flights is the main goal. On another hand, high-speed flight management in moreover congested airspace falls within the subject of safety. In conclusion, the discussed parameters strongly encourage the development of novel aircraft configurations to gain advantageous elements. The Scope Clause, on the other hand, is an agreement that places a cap on the number of aircraft seats in order to prevent outsourcing and guarantee the jobs of union pilots. Therefore, it is inevitable that the Modern Regional Jet (MRJ) fleet would grow. That demonstrates the importance of reliable flight control systems. In high-performance aerodynamic configurations, such as TBW aircraft, there are some re-raised interests [1, 2, 3]. Apart from that, the aviation industry has expressed interest in TBWs because of their fuel burn efficiency [4]. Despite considerable dynamic modeling research [5], it appears that no reliable auto-landing controller has been developed for these configurations.

Studies show that the landing procedure is the riskiest part of flying and calls for expert pilotage abilities. The International Civil Aviation Organization (ICAO) 6th annex document introduces three alternate aerodromes—Take-off, En-route, and Destination—where an MRJ shall land in the event of particular failure scenarios. In this case, [6] examined the most frequent causes of flying incidents and accidents during the approach phase. The most hazardous elements included are pilot erroneous decisions (74%), skipping or completing activities incorrectly (72%), and ineffective crew communication, mutual cooperation, and mutual control (63%). The cited elements strengthen the function of trendy autonomous controllers with great dependability to bolster safety. There are several studies with advanced control centralization in the landing procedure. For instance, [7] developed a double-loop nonlinear dynamic inversion controller based on a deep failure estimator made up of layers of Long-short Term Memory (LSTM) and Convolution Neural Networks (CNN). These neural networks were trained for severe

*Corresponding author

Email address: banazadeh@sharif.edu (Afshin Banazadeh)

stuck failures, with time-series data on landing trajectory patterns in actuator faulty and healthy landing condition simulations. In order to control the trajectory of a tailless and blended wing UAV confronting air turbulences and sensor measurement errors, a unique auto-landing framework was presented in [8]. In this research, a Backstepping-based controller is used to control the attitude angles. A Dynamic Inversion-based controller creates the throttle signal to keep a constant velocity, and an adaptive disturbance observer estimates the atmospheric turbulences to track the proposed landing trajectory. In [9] a generalized Anti-windup based on traditional PID controllers as well as a phase compensation system used to train a neural-assisted Sliding Mode controller. In order to tackle stuck actuator failures during an auto-landing scenario. It is demonstrated that the capacity of the neural-aided Sliding Mode controller to tolerate faults is greatly improved by adding Anti-windup and phase compensation. An aircraft heading angle is guided by a Deep Q-learning (DQL) in [10], allowing it to land in the desired 2-dimensional field. In this study, the dynamic modeling of aircraft is not included. In [11] a Deep Deterministic Policy Gradient (DDPG) was used to control an Unmanned Aerial Vehicle (UAV's) desired path for the landing flare phase in the longitudinal channel in existing wind disturbances. The structure of the proposed method includes two Deep ANNs as an Actor-critic architecture. Similar to this, the DDPG approach is employed in the outer loop of a landing procedure in [12] whereas the inner loop is controlled by a Proportional-integral-derivative (PID) controller. It is important to note that several classic techniques for aircraft attitude control have been created to improve the quality of landings. The main shortcoming of these traditional theories is their lack of adaptation in extended working points. To overcome this weakness, some existing approaches have increased their robustness by utilizing ANNs.

In this regard, publications like [13] and [14] are considered. In the first paper, a H_2 controller is addressed to actuator faults and wind disturbances. The focus of the second paper is on designing an online neural-aided controller to increase the robustness of existing controllers for fault tolerance. Although not specified in the landing phase, a different group of publications also deals with controller design. For instance, [15] presented a layered Model Predictive Control system based on simple sparse rapidly exploring random trees for path planning, path control, velocity control, and angular

velocity control. This method improved the estimation of a real-time, nonlinear, and onboard convex Flight-envelop calculation. For hydraulic actuator failures, [16] created an Integral Sliding Mode controller featuring Control Allocation. This controller eliminates the need to redesign another controller owing to distributing control signals among redundant actuators. An ANN-based adaptive controller using Feedback Linearization was developed in [17] to address the dramatic roll and unsteady longitudinal behavior in the condition of partial wing damage. In another study, to achieve hydraulic fault tolerance in the longitudinal axis, [18] evaluated the performance of three controllers, including Adaptive Back-stepping, Robust Sliding Mode, and PID. In this instance, the initial controller overcame the other methods. A Q-learning horizontal trajectory tracking controller with an ANN foundation was developed in [19] using the MDP model of an airship with fine stability characteristics. In this study, the method of action selection was optimized using a Cerebellar Model Articulation Controller (CMAC) neural network. A Soft Actor-critic (SAC) technique was used in [20] to solve a path planning problem for a Long-endurance, Solar-powered UAV that took energy consumption into account. Another study cited as [21] focused on a Skywalker X8 inner loop control employing SAC and comparing it with a PID controller.

Proximal Policy Optimization (PPO), was used in [22] for orientation control of a typical extremely dynamic coupled Fixed-wing aircraft in the stall circumstance. After 100,000 episodes, there was a successful convergence of the PPO. The efforts that have been mentioned thus far use ANNs to improve convergence and robustness. To the best of our knowledge, there are discrete RL-based attitude control studies without using ANNs. A Q-learning method was used in [23] to control longitudinal and lateral angles in a general aviation airplane (Cessna 172). This research controls the desired angles of zero and the airplane profits good stability characteristics.

There are some Fuzzy adaptations on [24] work like [25] where the Q-functions and action selection strategy are inferred from Fuzzy rules. Also, in order to reduce the number of states needed to shape an MDP model for mobile robots that avoid obstacles, [26] suggests a Fuzzy technique. Because the mobile robot may encounter an infinite number of different conditions. The Fuzzy method is used to generalize the condition and minimize processor requirements alongside reducing states. Also, [27] proposed a

dynamic Fuzzy Q-learning for online and continuous tasks in mobile robots. In [28], the Fuzzy Q-learning (FQL) method and Strictly Negative Imaginary (SNI) property are used to provide a novel robust adaptive control for quadrotor attitude and altitude stabilization. The objective is to develop a control strategy that dynamically adapts the SNI controller using FQL. Another study, [29] used Q-learning as an attitude controller for a unique, highly maneuverable regional jet aircraft in MDP and POMDP scenarios. The simulation results in a variable pitch angle tracking were satisfactory.

Motivated by the preceding discussions, the following are the main contributions of the current study:

1. A novel continuous action generator is developed as a general connector between every (discrete/continuous) optimal policy and the RL environment.
2. In response to worldwide aviation community expectations, a TBW aircraft (figure 1) with specific stability characteristics is selected for the auto-landing problem, where the high maneuverability of the aircraft brings significant challenges into the design process.
3. In contrast to many studies, the complexity of ANN architectures and the low adaptation of classic methods are well resolved using Fuzzy Q-learning.
4. The robustness and reliability of the proposed FQL are examined under different flight conditions consisting of sensor measurement noises, atmospheric disturbances, actuator faults, and model uncertainties.

2. Six-DoF Aircraft Dynamic Modeling

In order to develop a nonlinear RL environment, the 6-DoF nonlinear equations of motions cited in [30, 31] are utilized in this section. Many environments based on Gym and Flight Gear are open-source, such as GymFG ([32]). But this plant must model and simulate from scratch due to the unique characteristics of the innovative configuration. In this approach, it is presumed that the earth is flat. Consequently, the body frame translational and rotational equations are as follows:

$$mD^B \mathbf{v}^B + m\boldsymbol{\Omega}^B \mathbf{v}^B = \mathbf{f}_a^B + \mathbf{f}_p^B + m\mathbf{g}^B, \quad (1)$$

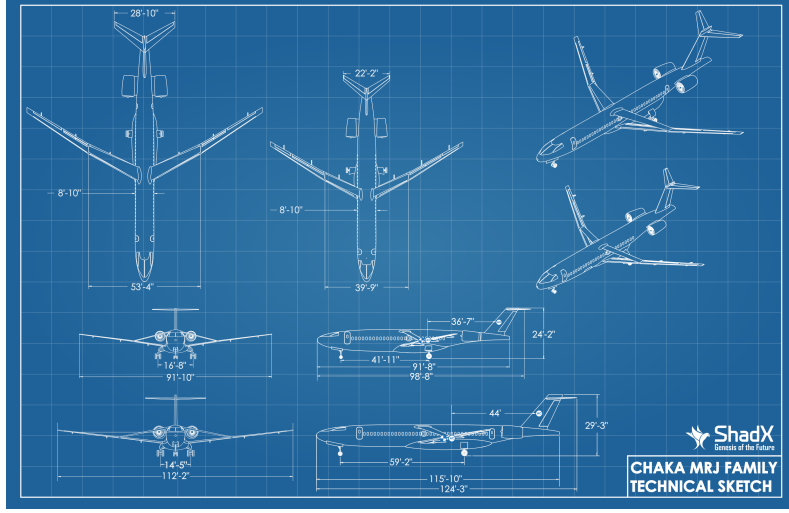


Figure 1: Chaka 50 and 76 Modern Regional Jet (MRJ) Family [4]

$$D^B(I^B \omega^B) + \Omega^B I^B \omega^B = m_a^B + m_p^B. \quad (2)$$

Where u, v, w are the velocity components, and D^B is defined as the Rotational Time Derivative in body frame. So the $D^B \mathbf{v}^B$ equals $[\frac{dv}{dt}]^B = [\dot{u} \ \dot{v} \ \dot{w}]^T$, and $[\omega]^B = [p \ q \ r]^T$ are the roll, pitch, and yaw angular rates vector in body frame. Also Ω^B is the skew-symmetric form of angular rates vector.

$$[\Omega]^B = \begin{bmatrix} 0 & -r & q \\ r & 0 & -p \\ -q & p & 0 \end{bmatrix}. \quad (3)$$

Furthermore, m is the mass of aircraft, and I^B is the moment of inertia matrix in body frame;

$$[I]^B = \begin{bmatrix} I_x & 0 & I_{xz} \\ 0 & I_y & 0 \\ I_{xz} & 0 & I_z \end{bmatrix}. \quad (4)$$

In equations (1) and (2), some variables on the right-hand side are considered to be zero including \mathbf{m}_p^B vector which is engine power moments. Also, \mathbf{f}_a^B , \mathbf{f}_p^B , and \mathbf{m}_a^B are considered as aerodynamic force, engine power force, and aerodynamic moment vectors. Where except engine power, the other non-zero forces and moments are computed in

aerodynamic frame as follows;

$$\begin{bmatrix} L \\ D \\ m_a \end{bmatrix}^S = \bar{q} S \bar{c} \begin{bmatrix} c_{L_0} & c_{L_\alpha} & c_{L_{\dot{\alpha}}} & c_{L_u} & c_{L_q} & c_{L_{\delta_E}} \\ c_{D_0} & c_{D_\alpha} & c_{D_{\dot{\alpha}}} & c_{D_u} & c_{D_q} & c_{D_{\delta_E}} \\ c_{m_0} & c_{m_\alpha} & c_{m_{\dot{\alpha}}} & c_{m_u} & c_{m_q} & c_{m_{\delta_E}} \end{bmatrix} \begin{bmatrix} 1 \\ \alpha \\ \frac{\dot{\alpha} \bar{c}}{2V_{P_1}} \\ \frac{u}{V_{P_1}} \\ \frac{q \bar{c}}{2V_{P_1}} \\ \delta_E \end{bmatrix}. \quad (5)$$

Furthermore, aerodynamic forces need a transfer from stability to the body frames of the angle of attack α around y_S axis.

$$\begin{bmatrix} f_{a_x} \\ f_{a_y} \\ f_{a_z} \end{bmatrix}^B = \begin{bmatrix} \cos \alpha & 0 & -\sin \alpha \\ 0 & 1 & 0 \\ \sin \alpha & 0 & \cos \alpha \end{bmatrix}^{BS} \begin{bmatrix} -D \\ 0 \\ -L \end{bmatrix}^S. \quad (6)$$

Also, the gravitational acceleration vector \mathbf{g}^B in the body frame is as follows:

$$\begin{bmatrix} g_x \\ g_y \\ g_z \end{bmatrix}^B = \begin{Bmatrix} -g \sin(\theta) \\ g \cos(\theta) \sin(\phi) \\ g \cos(\theta) \cos(\phi) \end{Bmatrix}. \quad (7)$$

Additionally, rotational kinematic equations are required for transfer from body to inertial frames.

$$\begin{bmatrix} \dot{\phi} \\ \dot{\theta} \\ \dot{\psi} \end{bmatrix} = \begin{bmatrix} 1 & \sin \varphi \tan \theta & \cos \varphi \tan \theta \\ 0 & \cos \varphi & -\sin \varphi \\ 0 & \sin \varphi / \cos \theta & \cos \varphi / \cos \theta \end{bmatrix} \begin{bmatrix} p \\ q \\ r \end{bmatrix}^B. \quad (8)$$

So, the translational kinematic equations using (1), and (8), in the inertial frame is achievable.

$$\begin{bmatrix} \dot{x} \\ \dot{y} \\ \dot{z} \end{bmatrix}^E = \begin{bmatrix} \cos \psi \cos \theta & \cos \psi \sin \theta \sin \varphi - \sin \psi \cos \varphi & \cos \psi \sin \theta \cos \varphi + \sin \psi \sin \varphi \\ \sin \psi \cos \theta & \sin \psi \sin \theta \sin \varphi + \cos \psi \cos \varphi & \sin \psi \sin \theta \cos \varphi - \cos \psi \sin \varphi \\ -\sin \theta & \cos \theta \sin \varphi & \cos \theta \cos \varphi \end{bmatrix} \begin{bmatrix} u \\ v \\ w \end{bmatrix}^B. \quad (9)$$

Based on Computational Fluid Dynamics (CFD), stability and control derivatives for the Chaka-50 are presented in [4]. Table (1) summarises these derivatives for two flying

scenarios. Trim conditions in a wings-level flight are calculated for simulation verification utilizing trim equations in [33]. The drag equation takes into account the absolute values of δ_E , i_{H_1} , and α_1 . In addition, the flight path angle γ_1 , motor installation angle ϕ_T , and horizontal tail incidence angle i_H are all equal to zero. By solving the trim equation, the elevator deflection δ_E and required thrust f_{a_x} for a trim flight are obtained and shown in table (2). The numbers in the aforementioned table (2) are crucial for the validation of the 6-DoF simulation.

Table 1: Stability and control derivatives of Chaka 50 MRJ (1/rad)

Longitudinal Derivatives	Ideal	Random Uncertainty ([-10 10])%	Longitudinal Derivatives	Ideal	Random Uncertainty ([-10 10])%
c_{D_0}	0.0338	0.0358	c_{L_u}	0.081	0.076
c_{L_0}	0.3180	0.3363	c_{m_u}	-0.039	-0.041
c_{m_0}	-0.06	-0.061	c_{L_q}	12.53	12.56
c_{D_α}	0.8930	0.893	c_{m_q}	-40.69	-37.27
c_{L_α}	14.88	14.52	$c_{D_{\delta_E}}$	0.1570	0.1483
c_{m_α}	-11.84	-11.84	$c_{L_{\delta_E}}$	0.78	0.74
c_{D_u}	0.041	0.373	$c_{m_{\delta_E}}$	-5.98	-5.93

2.1. Six-DoF Aircraft Dynamic Model considering Atmospheric Disturbances

Aircraft landing quality is affected by atmospheric disturbance which is air turbulence in the small areas of the atmosphere that often happens close to the ground. The

Table 2: Trim parameters of Chaka 50 MRJ

Parameter	Value
Required Thrust (f_{a_x})	21433.02 (lbs)
Required Elevator (δ_E)	0.39 (deg)
Angle of Attack (α)	-2.28 (deg)

Table 3: Chaka 50 MRJ specifics for simulation

Parameter	Value	Parameter	Value
Wing Area(m^2)	43.42	$I_{xx}(kg.m^2)$	378056.535
Mean Aerodynamic Chord(m)	1.216	$I_{yy}(kg.m^2)$	4914073.496
Span(m)	28	$I_{zz}(kg.m^2)$	5670084.803
Mass(kg)	18418.27	$I_{xz}(kg.m^2)$	0
Initial Speed $V_{P_1}(\frac{m}{s})$	160	Initial height $h_1(m)$	100

coordinates of disturbances that result in a loss of lift and altitude are the most hazardous since the aircraft is getting close to the final approach. The atmospheric disturbance is described in the literature as a stochastic process that is characterized by velocity spectra. There are two widely used models that are typically used in flight dynamic simulations: (1) Dryden Continuous Turbulence Model; and (2) Von Karman Continuous Turbulence Model

The Dryden atmospheric turbulence is used in this study for two reasons. First, it allows for easier mathematical modeling and covers both linear and rotational components of disturbance velocity.

$$\begin{aligned}
G_u(s) &= \sigma_u \sqrt{\frac{2L_u}{\pi u_1}} \left[\frac{1}{1 + (\frac{L_u}{u_1} s)} \right], \\
G_v(s) &= \sigma_v \sqrt{\frac{L_v}{\pi u_1}} \left[\frac{1 + 2\sqrt{3} \frac{L_v}{u_1} s}{(1 + \frac{2L_v}{u_1} s)^2} \right], \\
G_w(s) &= \sigma_w \sqrt{\frac{2L_w}{\pi u_1}} \left[\frac{1 + 2\sqrt{3} \frac{L_w}{u_1} s}{(1 + \frac{2L_w}{u_1} s)^2} \right],
\end{aligned} \tag{10}$$

where according to [34], L_w , L_v , and L_u are the scaling length;

$$\begin{aligned}
L_u = L_v &= \frac{z}{(0.177 + 0.000823z)^{1.2}}, \\
L_w &= z,
\end{aligned} \tag{11}$$

and σ_u , σ_v , and σ_w are the intensity of turbulence.

$$\begin{aligned}
\sigma_u = \sigma_v &= \frac{\sigma_w}{(0.177 + 0.000823z)^{0.4}}, \\
\sigma_w &= 0.1u_{20},
\end{aligned} \tag{12}$$

where wind speed at 20 feet is specified by u_{20} . The motion equations have now been modified to include the effects of the wind based on [35]. In general, the inertial frame is used to compute the wind and its derivatives. But complex computations are required for its transition into the body. As an alternative, one may use the derivatives in the body reference to reach; where the \mathbf{W}^B is the wind velocity vector in body frame; $[W]^B = [W_x \ W_y \ W_z]^T$.

$$\begin{aligned}\dot{W}_x &= \left[\frac{\partial W_x}{\partial x} \right]^B (u + W_x) + \left[\frac{\partial W_x}{\partial y} \right]^B (v + W_y) + \left[\frac{\partial W_x}{\partial z} \right]^B (w + W_z) + \left[\frac{\partial W_x}{\partial t} \right]^B, \\ \dot{W}_y &= \left[\frac{\partial W_y}{\partial x} \right]^B (u + W_x) + \left[\frac{\partial W_y}{\partial y} \right]^B (v + W_y) + \left[\frac{\partial W_y}{\partial z} \right]^B (w + W_z) + \left[\frac{\partial W_y}{\partial t} \right]^B, \\ \dot{W}_z &= \left[\frac{\partial W_z}{\partial x} \right]^B (u + W_x) + \left[\frac{\partial W_z}{\partial y} \right]^B (v + W_y) + \left[\frac{\partial W_z}{\partial z} \right]^B (w + W_z) + \left[\frac{\partial W_z}{\partial t} \right]^B.\end{aligned}\quad (13)$$

The spatial derivatives of the wind speed, which are often stated in the inertial frame, must be transferred to the body frames of reference in (13);

$$[\nabla W]^B = [T]^{BE} [\nabla W]^E [\bar{T}]^{BE}. \quad (14)$$

The effect of wind on angular rates ω_w^E can be defined as a rigid solid air caused by fluid stresses, and is expressed in the inertial frame as;

$${}^E = \frac{1}{2} \left[\left(\frac{\partial W_z}{\partial y} - \frac{\partial W_y}{\partial z} \right) \right]^E i + \frac{1}{2} \left[\left(\frac{\partial W_x}{\partial z} - \frac{\partial W_z}{\partial x} \right) \right]^E j + \frac{1}{2} \left[\left(\frac{\partial W_y}{\partial x} - \frac{\partial W_x}{\partial y} \right) \right]^E k. \quad (15)$$

The above equation must be transferred to the body axis so as to use in the 6-DoF equation;

$$\begin{bmatrix} p \\ q \\ r \end{bmatrix}^B = \begin{bmatrix} p \\ q \\ r \end{bmatrix}^B - [T]^{BE} \begin{bmatrix} \left(\frac{\partial W_z}{\partial y} - \frac{\partial W_y}{\partial z} \right) \\ \left(\frac{\partial W_x}{\partial z} - \frac{\partial W_z}{\partial x} \right) \\ \left(\frac{\partial W_y}{\partial x} - \frac{\partial W_x}{\partial y} \right) \end{bmatrix}^E. \quad (16)$$

2.2. Actuator Fault

A type of failure that affects the plant inputs is an actuator fault. Actuator faults in the aircraft might result from improper maintenance procedures, the age of the material, or improper operation. In this study, the actuator fault is expressed in two terms: the first, is a multiplicative term, which is the elevator's inability to achieve the required

amount, and the second, is an additive term, which is the output quantity bias.

$$\begin{aligned}\delta_{E_t} &= 0.3\delta_{E_t} - 0.7^\circ, & \text{If } t > 12s, \\ &0.4\delta_{E_t} + 0.6^\circ, & \text{If } 12s > t > 8s, \\ &0.5\delta_{E_t} - 0.5^\circ, & \text{If } 8s > t > 4s.\end{aligned}\tag{17}$$

According to equation (17), the elevator operates with 30% power and concurrently biases its output by -0.7° after 12 seconds of flight because it is anticipated that the issue would worsen over time. After 4 and 8 seconds of flight, identical faults with different parameter values will have occurred. In this study, 50% deficiency and 60° additive bias after 4 seconds and 30% deficiency and 0.6° additive bias after 8 seconds were taken into consideration.

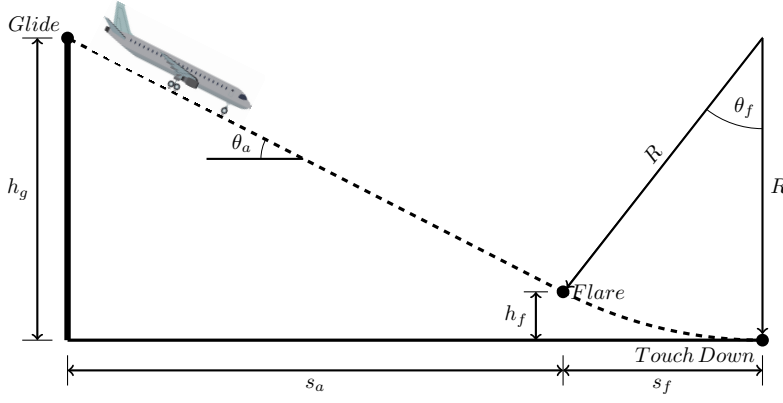


Figure 2: Landing Path and Landing Distance Diagram

3. Landing Path Planning

Examining Figure 2, the desired approach angle is $\theta_a \leq 3$ according to [36]. In this case assuming aircraft speed in touch down point $V_{TD} = 1.15V_{stall}$, and also speed in flare zone $V_f = 1.23V_{stall}$. So, the formula of flare circular arc is:

$$R = \frac{V_f^2}{0.2g}.\tag{18}$$

Now, in order to calculate θ_f in each time-step, flare altitude h_f is required.

$$h_f = R - R \cos \theta_a.\tag{19}$$

By considering aforementioned formulas, the approach distance s_a , and the flare distance s_f are as follows:

$$s_a = \frac{-(50 - h_f)}{\tan \theta_a}, \quad (20)$$

$$s_f = -R \sin \theta_a. \quad (21)$$

Also, by using the formula $s_{td} = s_a + s_f$ to represent touch-down distance, the desired θ_f at each time step after covering approach distance is produced by:

$$\theta_f = \arcsin\left(\frac{x - x_{td}}{R}\right). \quad (22)$$

4. Dynamic Inversion Auto Landing Structure

Consider the following formulation to represent the nonlinear dynamic system:

$$\begin{aligned} \dot{\mathbf{x}} &= \mathbf{f}(\mathbf{x}) + \mathbf{g}(\mathbf{x})\mathbf{u}, \quad \mathbf{x}(0) = \mathbf{x}_0, \\ \mathbf{y} &= \mathbf{h}(\mathbf{x}), \end{aligned} \quad (23)$$

where $\mathbf{x} \in \mathbf{R}$, $\mathbf{y} \in \mathbf{R}$, $\mathbf{u} \in \mathbf{R}$ are the vector of state, measurement output, and control input. The goal of the problem is often to design a suitable \mathbf{u} such that \mathbf{y} tracks desired \mathbf{y}_{des} . By differentiating the output vector \mathbf{y} with respect to the state vector \mathbf{x} , this would be accomplished.

$$\dot{\mathbf{y}} = \frac{\partial \mathbf{h}}{\partial \mathbf{x}} \frac{d\mathbf{x}}{dt} = \frac{\partial \mathbf{h}}{\partial \mathbf{x}} \mathbf{f}(\mathbf{x}) + \frac{\partial \mathbf{h}}{\partial \mathbf{x}} \mathbf{g}(\mathbf{x})\mathbf{u}. \quad (24)$$

The error between \mathbf{y} and \mathbf{y}_{des} must be eliminated by establishing a first-order dynamic error, which is defined as $\mathbf{e}_y = \mathbf{y} - \mathbf{y}_{des}$:

$$\begin{aligned} \dot{\mathbf{e}}_y + \mathbf{K}\mathbf{e}_y &= 0, \\ \dot{\mathbf{y}} - \dot{\mathbf{y}}_{des} + \mathbf{K}(\mathbf{y} - \mathbf{y}_{des}) &= 0. \end{aligned} \quad (25)$$

The error can be exponentially reduced by calculating the preceding equation while assuming that \mathbf{K} is a positive definite matrix. Let assume $\mathbf{F}_y(\mathbf{x}) = \frac{\partial \mathbf{h}}{\partial \mathbf{x}} \mathbf{f}(\mathbf{x})$, $\mathbf{G}_y(\mathbf{x}) = \frac{\partial \mathbf{h}}{\partial \mathbf{x}} \mathbf{g}(\mathbf{x})$ and $\mathbf{g}(\mathbf{x})$ as an invertible matrix to derive the control signal as follows:

$$\mathbf{u} = [\mathbf{G}_y(\mathbf{x})]^{-1}[\dot{\mathbf{y}} - \mathbf{F}_y(\mathbf{x})]. \quad (26)$$

By substituting $\dot{\mathbf{y}}$ as a function of \mathbf{e} :

$$\mathbf{u} = [\mathbf{G}_y(\mathbf{x})]^{-1}[\dot{\mathbf{y}}_{des} - \mathbf{K}(\mathbf{y} - \mathbf{y}_{des}) - \mathbf{F}_y(\mathbf{x})]. \quad (27)$$

The main challenge is assigning \mathbf{K} for error reduction. Extreme non-linearity, couplings, modeling uncertainty, and aerodynamic uncertainty combined with atmospheric disturbances lead to adaptive \mathbf{K} designation in this problem, which increases complexity. In this section, the Dynamic Inversion controller was developed based on [37]. According to aforesaid theories, first-order error in outer loop is considered $\dot{e}_h + k_h e_h = 0$, where $e_h = h - h_{des}$. So the desired path angle is expressed as:

$$\theta_{des} = \arcsin\left(\frac{\dot{h}_{des} - k_h(h - h_{des})}{\sqrt{a_h^2 + b_h^2}}\right) - \arctan\left(\frac{b_h}{a_h}\right), \quad (28)$$

where $a_h = u$, and $b_h = v \sin \phi + w \cos \phi$. Then for inner loop control, the first-order error is used respectively. So;

$$\dot{\theta} - \dot{\theta}_{des} + k_\theta(\theta - \theta_{des}) = 0. \quad (29)$$

Obviously, forces and moments are applied to aircraft in body axis.

$$q_{des} = \sec \phi(\dot{\theta}_{des} - k_\theta(\theta - \theta_{des}) + r \sin \phi). \quad (30)$$

Now the control of q in order to track q_{des} is applicable. So the first-order error is applied:

$$\dot{q} - \dot{q}_{des} + k_q(q - q_{des}) = 0. \quad (31)$$

By driving \dot{q} in equation (1) and substituting equation (31), the desired longitudinal control input δ_E is accessible.

$$\delta_E = \frac{I_y(\dot{q}_{des} - k_q(q - q_{des})) + (I_x - I_z)rp - M_A - M_{\delta_E}\delta_E}{M_{\delta_E}}, \quad (32)$$

where $M_{\delta_E} = \bar{q}S\bar{c}c_{m_{\delta_E}}$.

Remark: It is apparent that the elevator deflection computation needs to desired pitch angle and desired pitch rate states. But in the FQL method, it will be seen later that the control signals are computed by just the desired pitch angle state during the trajectory tracking phase.

5. Fuzzy Q-learning Auto-landing Structure

Because of their narrow Mean Aerodynamic Chord (MAC), TBW aircraft typically exhibit insufficient longitudinal stability. More specifically, this finding may be confirmed

by evaluating the Phugoid and Short-period modes of the Boeing N+3 TTBW [5] and Chaka 50 against the Cessna 172 [38]. Table (4) contains an overview of the numerical data for the longitudinal modes of the aforementioned transport aircraft. This table can support the claim made above. To be clear, due to their superior manoeuvrability, the Chaka and Boeing, which have similar designs, experience poor longitudinal stability qualities. The Cessna 172, on the other hand, benefits from stable dynamics behaviour. For clarification, the damping ratio of the Chaka 50's Phugoid mode causes low-stability behavior resulting in long-term oscillations as depicted in [29].

Table 4: Longitudinal Dynamics Characteristic

Aircraft Roots	Short Period Roots	Phugoid Roots
Chaka 50	$-0.8 \pm 0.61i$	$-0.0064 \pm 0.05i$
Cessna 172	$-3.23 \pm 5.71i$	$-0.025 \pm 0.19i$
Boeing N+3	$-0.35 \pm 0.35i$	$-0.0082 \pm 0.07i$

5.1. MDP Definition in Auto-landing

A sequential decision-making process, such as an auto-landing problem, must be formalized as MDPs since one action affects not only the next state and its immediate reward but also forthcoming states and their future rewards [39]. To be clear, at each time-step t , the controller receives an state observation from the 6-DoF simulation, including $\theta_t \in \mathbf{S}_1$ and $\dot{\theta}_t \in \mathbf{S}_2$. Based on it, the controller specifies an action, $\delta_{E_t} \in \mathbf{A}(\mathbf{s})$, which is the elevator deflection. The simulation runs, and in the following time step $t+1$, the controller receives a reward $R_{t+1} \in \mathbf{R}$ to assess its performance and find itself in the next state $\theta_{t+1}, \dot{\theta}_{t+1}$ until reaching to terminal state $\theta_T, \dot{\theta}_T$.

$$\theta_0, \dot{\theta}_0, \delta_{E_0}, R_1, \theta_1, \dot{\theta}_1, \delta_{E_1}, R_2, \dots, \theta_T, \dot{\theta}_T. \quad (33)$$

Here, θ_0 , and $\dot{\theta}_0$ are the initial states, and δ_{E_0} is the initial elevator deflection, moreover R_t defines the instant reward at time-step t . A random pick of R_t , θ_t , and $\dot{\theta}_t$ have a clear discrete probability distribution that is solely reliant on the past state-action in this issue. Thus, by treating θ_t and $\dot{\theta}_t$ as states, the Markov property is satisfied because

they contain complete information about all aspects of the controller-aircraft (agent-environment) interaction history that matter in the future. So, for all $\theta_c, \theta_p \in \mathbf{S}_1$, $\dot{\theta}_c, \dot{\theta}_p \in \mathbf{S}_2$, and $\delta_E \in \mathbf{A}(\mathbf{s})$, the equation of the MDP problem is defined as P ;

$$P(\theta_c, \dot{\theta}_c \mid \theta_p, \dot{\theta}_p, \delta_E) = Pr\{\theta_t = \theta_c, \dot{\theta}_t = \dot{\theta}_c \mid \theta_{t-1} = \theta_p, \dot{\theta}_{t-1} = \dot{\theta}_p, \delta_{E_t} = \delta_E\}, \quad (34)$$

where c and p are used for the current state and the previous state, respectively. In this problem, according to table (5), equation (34) always has a deterministic numerical amount in $[0 \ 1]$ for all states. All states are well-defined and each receives a distinct reward.

$$\sum_{\theta_c \in \mathbf{S}_1} \sum_{\dot{\theta}_c \in \mathbf{S}_2} P(\theta_c, \dot{\theta}_c \mid \theta_p, \dot{\theta}_p, \delta_E) = 1. \quad (35)$$

The goal of finite MDP is to design a policy that maximizes reward over time. To find an optimal policy for taking δ_E in state $\theta, \dot{\theta}$, the state-action value function $\mathbf{Q}_\pi(\theta, \dot{\theta}, \delta_E)$ must be maximized, which is defined as the expected return as the sum of discounted instant rewards by starting from one specific state and pursuing policy π to terminal state $\theta_T, \dot{\theta}_T$:

$$\mathbf{Q}_\pi(\theta, \dot{\theta}, \delta_E) = \mathbb{E}_\pi \left[\sum_{k=0}^{\infty} \gamma^k R_{t+k+1} \mid \theta_t = \theta, \dot{\theta}_t = \dot{\theta}, \delta_{E_t} = \delta_E \right], \quad (36)$$

where $0 < \gamma < 1$ is the discount factor, whereas $\gamma \simeq 0$ denotes the agent nearsightedness, and $\gamma \simeq 1$ means the agent is long-sighted.

5.2. Structure of Fuzzy Q-learning Controller

In the current study, Q-learning, an early breakthrough in Reinforcement Learning, is used to directly approximate the optimal elevator selection policy in each condition [24]. Q-Learning is an off-policy, model-free control algorithm based on the Temporal Difference (TD) method. In general, the system state $(\theta_t, \dot{\theta}_t)$ is obtained each time step, and by using the current elevator command (δ_{E_t}) the action selection policy will be updated. Because of the highly nonlinear and poor stability characteristics of TBW aircraft, the Q-learning implementation results can be unsatisfactory without employing continuous state-action [29]. Accordingly, two Q-tables are trained by the Fuzzy and basic Q-learning methodologies. Then, they are Incorporated in different auto-landing scenarios through a novel technique namely the Fuzzy Action Assignment (FAA), which can be introduced

as a general connector between various trained Q-tables and continuous environments. Instead of computing a discrete greedy action in a particular state $\theta, \dot{\theta}$, FAA technique assigns a relative weight (also defined as the validity function or membership function) to each cell of the grid of system states (see Figure 3). This assignment is performed based on the current value of the state-action value function. The membership function of each grid cell with centers θ_i and $\dot{\theta}_j$ is described as follows:

$$MF_{i,j} = \exp\left(-\frac{1}{2}\left(\frac{\theta_t - \theta_{i_t}}{\sigma_\theta}\right)^2\right) \exp\left(-\frac{1}{2}\left(\frac{\dot{\theta}_t - \dot{\theta}_{j_t}}{\sigma_{\dot{\theta}}}\right)^2\right), \quad (37)$$

where σ_θ , and $\sigma_{\dot{\theta}}$ define the validity widths of the membership functions. In this study, the elevator commands of TBW aircraft are specified into -0.25 to $+0.25$ radians with 0.025 intervals, corresponding to 21 elevator deflections. Also, the ϵ -greedy action selection strategy with epsilon decay is utilized in this research so as to select greedy elevator commands in the last episodes (when the trained policy is near-optimum).

$$\delta_{E_t} = \begin{cases} \arg \max_{\delta_E} Q(\theta_t, \dot{\theta}_t, \delta_E) & \text{with probability } 1 - \epsilon \\ \text{random action} & \text{with probability } \epsilon \end{cases} \quad (38)$$

Following that, δ_E is determined using a weighted average of neighbor membership functions at each time step as regards:

$$\delta_{E_t} = \frac{\sum_i \sum_j MF_{i,j_t} \arg \max_{\delta_E} Q(\theta_{i_t}, \dot{\theta}_{j_t}, \delta_E)}{\sum_i \sum_j MF_{i,j_t}}. \quad (39)$$

The computed elevator deflection is applied to the aircraft 6-DoF simulation environment and receives a scalar reward signal as performance feedback which is defined in the Reward Function Definition section.

5.2.1. State-action Value Function Updating Rule

In this study, the state-action value function directly estimates the optimal Q-table controller which is performed over episodes utilizing Fuzzy rules. The base updating rule equation is unchanged but the calculation of its different parts is improved dramatically. So in this part, the updating formalization of the terms of updating function is discussed. In this case, Q_f defines as the value of state-action in the previous time step that is

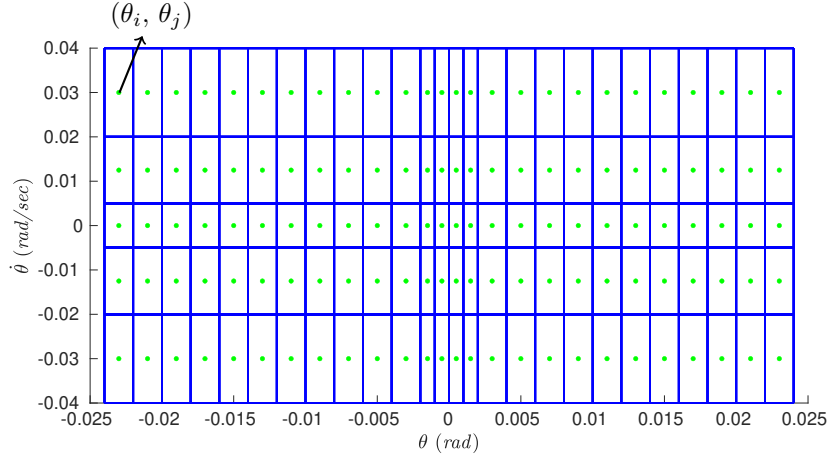


Figure 3: Grid of state variables used for tabular Q-learning (The center of each cell, which is used to compute the membership function of the cell is shown by a circle point.)

computed with its neighbor grids as:

$$Q_f(\theta_t, \dot{\theta}_t, \delta_{E_t}) = \frac{\sum_i \sum_j MF_{i,j_t} Q(\theta_{i_t}, \dot{\theta}_{j_t}, \delta_{E_t})}{\sum_i \sum_j MF_{i,j_t}}. \quad (40)$$

Then, estimating the optimal state-action value of the next time step using a Fuzzy scheme is important in order to, find an estimation of a sequence of best elevator deflection values that will be selected from that state until the terminal state. But note that the quota of neighbor elevators is seen using the membership function. The reason for this computation is obvious. The effect of one specific δ_E is not only on one pair of $\theta, \dot{\theta}$ but also has a nearly similar effect on their near neighbors. So the Fuzzy optimal future value is as follows;

$$\max_{\delta_E} Q_f(\theta_{t+1}, \dot{\theta}_{t+1}, \delta_E) = \frac{\sum_i \sum_j MF_{i,j_{t+1}} \max_{\delta_E} Q(\theta_{i_{t+1}}, \dot{\theta}_{j_{t+1}}, \delta_E)}{\sum_i \sum_j MF_{i,j_{t+1}}}, \quad (41)$$

where the membership function is related to the next time-step. Another step is to calculate the Temporal Difference (TD) in Fuzzy format. Therefore, the TD formulation is as follows;

$$TD_{i,j_t} = \frac{\sum_i \sum_j MF_{i,j_t} \left[R_{t+1} + \gamma \max_{\delta_E} Q_f(\theta_{t+1}, \dot{\theta}_{t+1}, \delta_E) - Q_f(\theta_t, \dot{\theta}_t, \delta_{E_t}) \right]}{\sum_i \sum_j MF_{i,j_t}}, \quad (42)$$

where the membership function in this step is related to the previous time-step. The pseudocode of the proposed control strategy is summarized in Algorithm 1.

5.2.2. Fuzzy Action Assignment Structure

As discussed earlier, the FAA receives optimal policies produced by various continuous or discrete RL algorithms. Then generates continuous actions for different control problems based on Fuzzy methodologies. Its implication are easy-going using just two equations 37, and 39. The pseudocode of FAA is explained in algorithm 2.

5.2.3. Reward Function Definition

The definition of an appropriate reward function is critical to the learning processes' convergence. Therefore, the reward function design and hyper-parameter adjustment have received significant attention in this study likewise. In this manner, the reward function is generated in three phases and comprises plant states such as θ, q, δ_E .

To begin with, in order to limit the elevator's high-frequency deflecting, severe penalties in the case of aggressive elevator selection are required. This penalty is performed whenever an elevator changes more than 0.1 radians.

$$R_t = -10000, \quad \text{If } (|\delta_{E_t}| - |\delta_{E_{t-1}}|) > 5.73^\circ. \quad (43)$$

The reward function will then be calculated as follows if the aircraft is close to the desired angle and the elevator operation frequency is reasonable.

$$\begin{aligned} R_t = & (300, \quad \text{If } |e_{\theta_t}| < 0.05^\circ), \\ & + (300, \quad \text{If } |e_{\theta_t}| < 0.02^\circ), \\ & + (400, \quad \text{If } |q_t| < 0.04^\circ), \\ & + (600, \quad \text{If } |q_t| < 0.02^\circ), \\ & + (800, \quad \text{If } |q_t| < 0.005^\circ), \end{aligned} \quad (44)$$

where $e_{\theta_t} = \theta_t - \theta_{des}$ is the proportional error. This definition first examines the state of pitch tracking. The controller then detects and prioritizes fewer pitch rates using higher reward allocations in the last episodes. The concepts stated above were defined for learning convergence. In other words, they are activated when the pitch angles are near the desired values. However, it is essential to guide the learning process in early episodes

with another phrase. As a result, if none of the above two requirements are satisfied, we should urge the air vehicle to proceed at the desired angle. Using the following reward function, this demand is achievable:

$$R_t = -(100 \times |e_{\theta_t}|)^2 - (40 \times |q_t|)^2. \quad (45)$$

As a result, the further the system deviates from the desired state, the lower the reward. In addition, to avoid excessive pitch rates, a derivative term (the second term) has been added into reward function. More specifically, the presence of the pitch rate (q_t) in equation (44), as well as its weight in equation (45), influences the convergence rate significantly.

6. Simulation Results and Discussion

The auto-landing control of an innovative TBW regional jet aircraft is developed utilizing Fuzzy Q-learning (FQL). The development process and the justification of the findings will therefore be touched upon in this section. The procedure is divided into two segments, as will be detailed later. The first is the learning phase, and the second is the trajectory tracking phase, which is the execution of the optimal policy. The proposed approach is then compared with Dynamic Inversion, a well-known robust control method according to studies. A novel continuous action selection method is developed in this study to function as a useful link between every trained Q-table and environment, as shown in figure 4.

In the learning phase, the desired pitch angle is set to 1 degree, and the initial pitch angle is selected as a random number between 0 and 2 degrees during episodes. The observation vector contains the pitch angle θ , and pitch rate (q) in each time step. Furthermore, the pitch and pitch angle rate state intervals are defined as a 3D table alongside with action vector (Elevator deflection intervals) which are located in the policy block. This block selects an action based on the ϵ -greedy strategy. The FQL core receives the reward, observation vector, and the relevant states of the pitch angle and pitch rate from the policy block (Figure 4) and updates the policy based on the aforementioned algorithm 1. Also, Q-learning receives all mentioned signals except the observation vector for policy updating.

Algorithm 1: Fuzzy Q-learning Aircraft Attitude Controller

Data: Learning Rate α , Discount Factor γ , Desired Angle $\theta_{des} = 1\text{deg}$, Validity

Widths $\sigma_\theta, \sigma_{\dot{\theta}}$, Elevator Deflections δ_E , Pitch (Rate) Angle Intervals $\theta, \dot{\theta}$.

Result: $Q_{\pi^*}(\theta, \dot{\theta}, \delta_E)$

```
1  $Q(\theta_0, \dot{\theta}_0, \delta_{E_0}) \leftarrow 0$ ; for all  $\theta \in \mathcal{S}_1, \dot{\theta} \in \mathcal{S}_2, \delta_E \in \mathcal{A}(\mathbf{s})$ ;  
2 for Episode Number = 1 to 20000 do  
3   Initialize 6-DoF simulation with a random  $\theta_0 \in [0 \ 2]$  deg.  
4   for time-step (0.01) = 0 to 5 sec do  
5     if  $\epsilon < \text{random number} \in [0 \ 1]$  then  
6        $\delta_{E_t} \leftarrow \text{random } \delta_E \in \mathcal{A}(\mathbf{s})$ ;  
7     else  
8       for  $i, j = 1$  to length  $I, J$  do  
9          $MF_{i,j_t} \leftarrow$  Compute membership function eq 37;  
10         $\delta_{E_t} \leftarrow$  Compute  $\delta_{E_t}$  eq 39;  
11      end  
12    end  
13    Execute 6-DoF simulation using computed  $\delta_{E_t}$ , observe  $R_{t+1}, \theta_{t+1}, \dot{\theta}_{t+1}$ ;  
14    for  $i, j = 1$  to length  $I, J$  do  
15       $MF_{i,j_{t+1}} \leftarrow$  Compute membership function eq 37;  
16       $Q_f(\theta_t, \dot{\theta}_t, \delta_{E_t}) \leftarrow Q(\theta_t, \dot{\theta}_t, \delta_{E_t})$  Computed by eq 40;  
17       $\max_{\delta_E} Q_f(\theta_{t+1}, \dot{\theta}_{t+1}, \delta_E) \leftarrow \max_{\delta_E} Q(\theta_{t+1}, \dot{\theta}_{t+1}, \delta_E)$  Computed by eq  
      41;  
18       $Q(\theta_{i_t}, \dot{\theta}_{j_t}, \delta_{E_t}) \leftarrow Q(\theta_{i_t}, \dot{\theta}_{j_t}, \delta_{E_t}) + \alpha \left[ TD_{i,j_t} \right]$  Based on eq 42;  
19    end  
20    Substitute simulation parameters in time-step  $t$  with  $t + 1$ .  
21  end  
22 end  
23 Return  $Q_{\pi^*}(\theta, \dot{\theta}, \delta_E)$ 
```

Algorithm 2: Fuzzy Action Assignment Scheme

Data: $Q_{\pi^*}(\theta, \dot{\theta}, \delta_E)$

Result: Continuous Elevator Deflection δ_E

- 1 Initialize 6-DoF simulation using predefined initial conditions;
- 2 **for** *time-step* $(0.01) = 0$ to 5 sec **do**
- 3 **for** $i, j = 1$ to length I, J **do**
- 4 $MF_{i,j_t} \leftarrow$ Compute membership function eq 37;
- 5 $\delta_{E_t} \leftarrow$ Compute δ_{E_t} eq 39;
- 6 **end**
- 7 Execute 6-DoF simulation using computed δ_{E_t} , compute the next system states;
- 8 Substitute simulation parameters in time-step t with $t + 1$.
- 9 **end**

The second phase is specified for the auto-landing control. In this case, the path planning block generates desired pitch angle in each time step. Then, one of the controllers out of three generates elevator signals. The output of the Fuzzy Q-table and Q-table is sent to the FAA block to produce continuous action (elevator deflections) based on algorithm 2. Several scenarios are defined in this stage including actuator faults, model uncertainties, and atmospheric disturbance plus sensor measurement noise. The parameters required for simulation are gathered in table 5. The positive part of pitch angle and pitch rate intervals are not mentioned in this table because of considering similar intervals. Useful to mention that all steps are developed in MATLAB R2022a and the PC is characterized by an 8 cores processor with 2.30 GHz, and 8 GiB RAM.

The learning results of the two methods are shown in figure 5. The main difference between MDP and POMDP models is observing the pitch rate in the MDP problem definition which in the POMDP is omitted. Obviously, the FQL conquered in comparison with Q-learning, and this insignificant difference will prove the robustness of the FQL later. Furthermore, its fluctuations are less than Q-learning (MDP). The POMDP policy is not included in the trajectory tracking phase owing to its unsuccessful findings [29]. The results of attitude tracking are gathered in figure 6. The first row is specified for

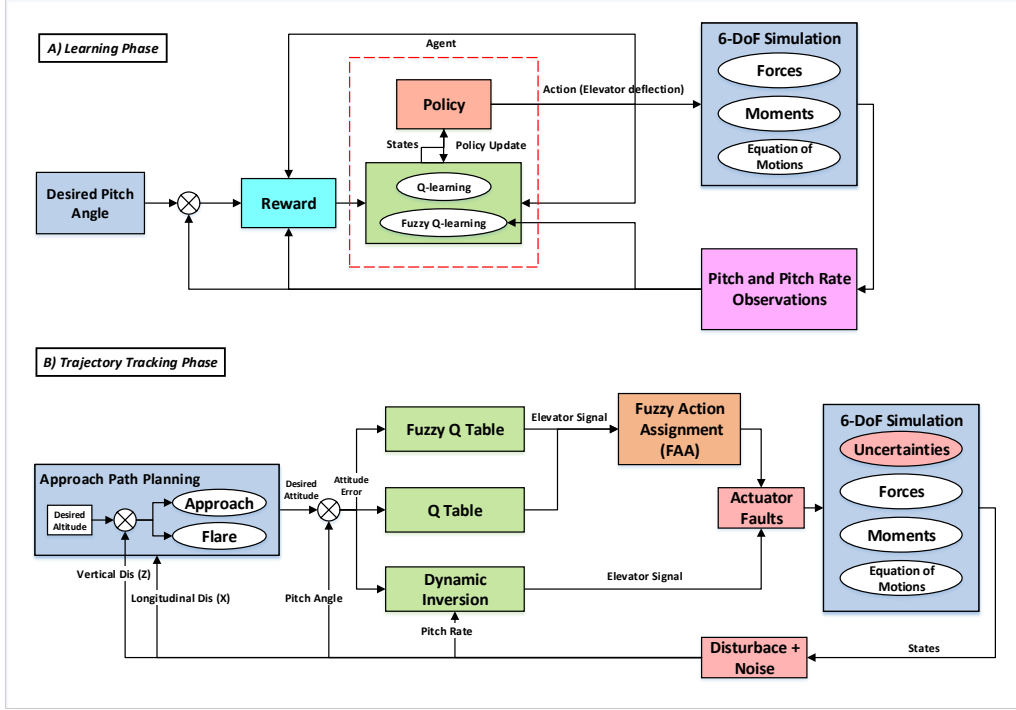


Figure 4: Block diagram of learning and trajectory tracking phases of all 3 methods

ideal flight conditions. All three methods were prosperous to track the desired angle. But the main difference is related to attitude tracking errors (TE_θ), altitude tracking errors (TE_h), and control effort (CE) which are defined as follows;

$$TE_\theta = \frac{\int_0^t |\theta_t - \theta_{des}| dt}{t}, \quad (46)$$

$$TE_h = \frac{\int_0^t |h_t - h_{des}| dt}{t}, \quad (47)$$

$$CE = \frac{\int_0^t |\delta_{E_t}| dt}{t}. \quad (48)$$

The second row contains simulation results in atmospheric disturbance and sensor measurement noise. The DI and FQL are able to track tough high-frequency responses. Although the path-planning block tried to generate less desired pitch angles to guide the aircraft to the desired trajectory, the QL diverged. The third row includes the results of actuator faults and finally, the last row gathers the results of model parameter

uncertainties which the performance of all controllers are reasonable.

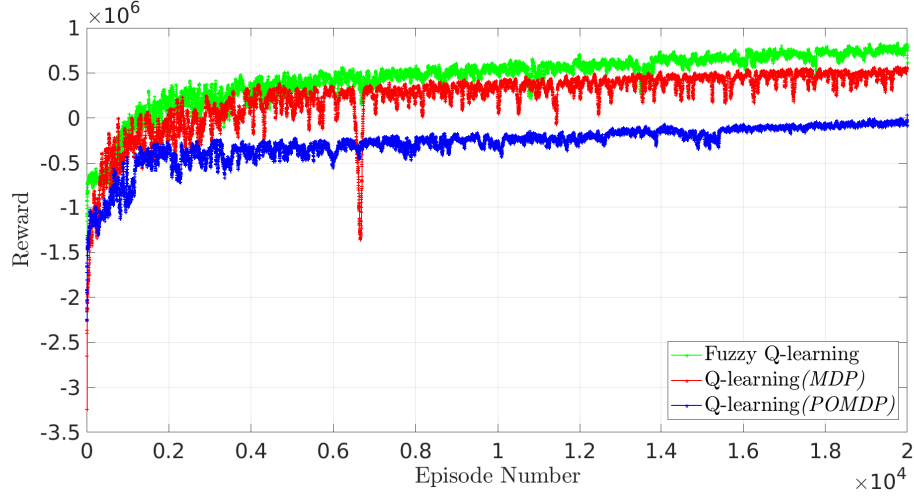


Figure 5: Learning result of Q-learning and Fuzzy Q-learning during 20000 Episodes

According to figure 7, the elevator deflection of all three methods explains significant data. To clarify, the first subplot indicates a larger initial deflection for DI in ideal flying conditions than the others. Furthermore, the second subplot demonstrates the poor performance of DI in the face of sensor noise and atmospheric disturbances. This result may be successful in trajectory tracking but is unable to be applicable. The third subplot is drawn for faulty elevator deflections with conspicuous jumps in all schemes. Finally, in contrast to the first subplot, the last subplot yields roughly analogous findings. It is useful to note that the DI overshoot before 10 seconds demonstrates its sensitivity to the commencing flare phase.

The next figure 8 demonstrates the altitude tracking of all three controllers. In an overview, the first, third, and last subplots prove the robustness of all three methodologies theoretically. But the second subplot is an exception. The QL controller is unable to accomplish its task properly but the FQL and DI have reasonable findings although the performance of DI is not useful for real applications. However, it is noticeable that the altitude tracking error of FQL in the middle of the approach distance is larger than DI. But during the flare phase that is more critical, the story changes, where the FQL surpasses DI.

Table 5: Controller parameters in learning and tracking phases

Parameter	Definition	Value
Epsilon(ϵ)	Exploration Probability	$[0.1 : 3e-6 : 0.04]$
Alpha(α)	Learning Rate	$[0.02 : 9e-7 : 0.002]$
Gamma(γ)	Discount Factor	0.99
Episode number	-	20000
$\theta(\text{rad})$	Pitch Angle Intervals	$[-10, -0.024 : 0.002 : -0.002, -0.001, 0]$
$\dot{\theta}(\text{rad})$	Pitch Rate Intervals	$[-10, -0.04, -0.02, -0.005]$
I	Adjacent pitch grids	$[i - 2 : i + 2]$
J	Adjacent pitch rate grids	$[j - 2 : j + 2]$
k_h	Altitude Control Coefficient	1.3
k_θ	Pitch Control Coefficient	5
k_q	Pitch Rate Control Coefficient	10

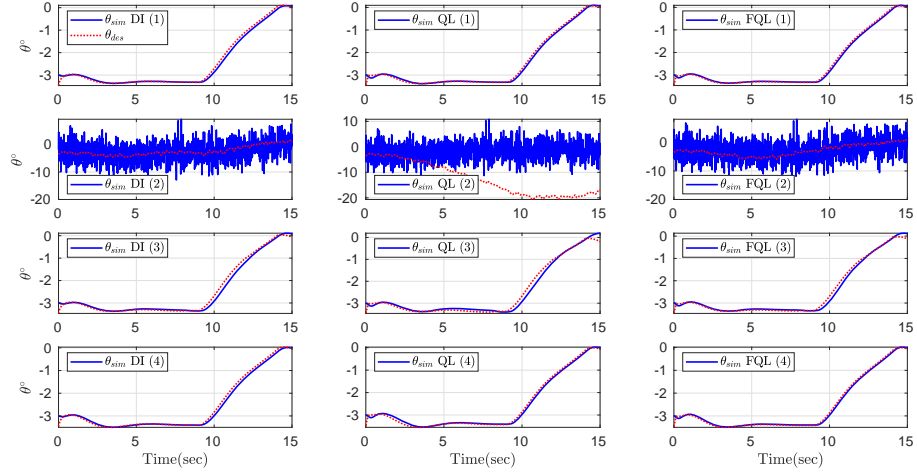


Figure 6: Attitude tracking of all 3 methods in (1) Ideal flight conditions (2) Atmospheric disturbance and sensor measurement noise (3) Actuator faults (4) Model parameters uncertainties.

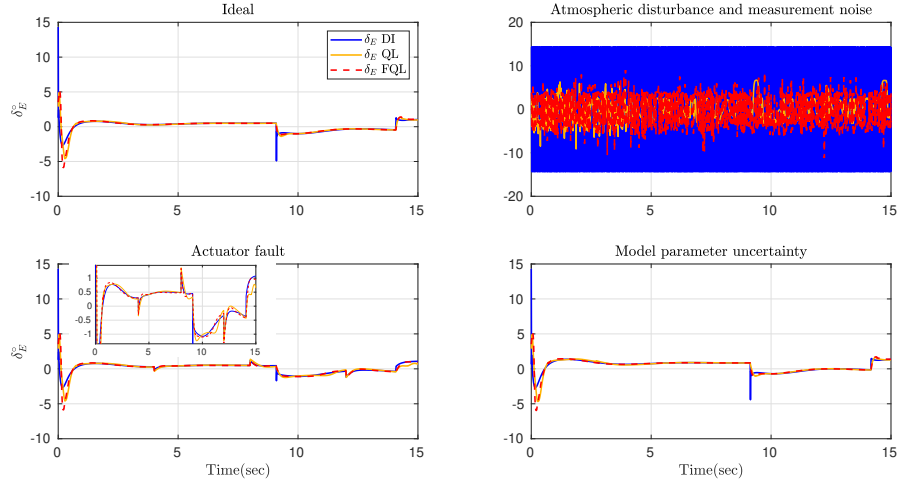


Figure 7: Computed elevator deflections of all 3 methods in different flight conditions

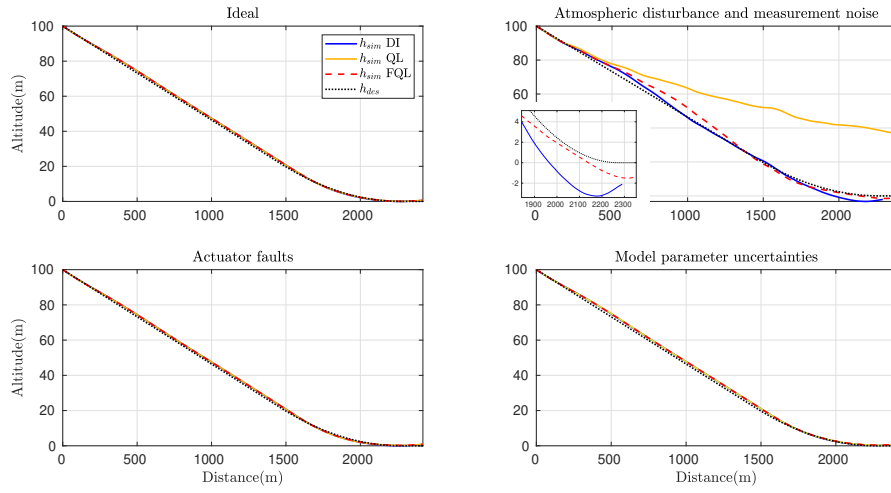


Figure 8: Altitude tracking of all 3 methods in various scenarios

The angle of attack (AoA) results of 15 seconds flight simulations are shown in figure 9. The less magnitude of AoA changes is clear in the first subplot compared to others. After the first subplot, the actuator faults have less influence on AoA although, there are some little jumps. The second subplot demonstrates an AoA change between -1 to 1 degree which is more than others despite its noisy specificity. This can amplify the drag where its consequences are clear in the next figure. Generally, the effect of actuator faults on AoA is less than model uncertainties.

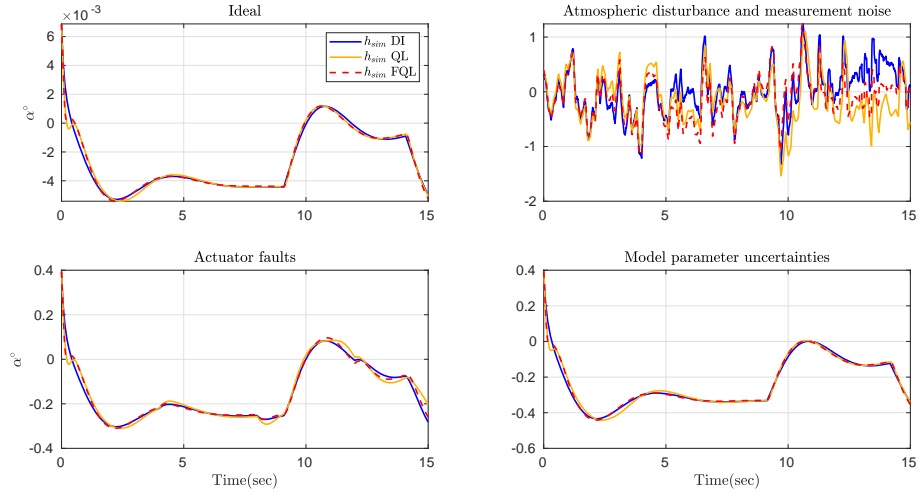


Figure 9: Aircraft Angle of Attack results in different flight simulations

The last figure depicts the speed of the airplane along its longitudinal body axis. According to the path planning section, the speed of aircraft at the touch-down point should be $161 \frac{m}{sec}$. The simulation of all flight conditions yields satisfactory results, however, the second subplot reveals a problem with DI. The performance of this controller leads the aircraft speed to stall margin, and the authors attribute this occurrence to high drag production caused by the elevator.

A summary of results is gathered numerically in table 6 for better comprehension. At a first glance, the superiority of FQL is noticeable in attitude tracking of all flight conditions except in presence of noise and disturbance where DI depicts better findings apparently. But the performance of DI in this circumstance is called into question owing

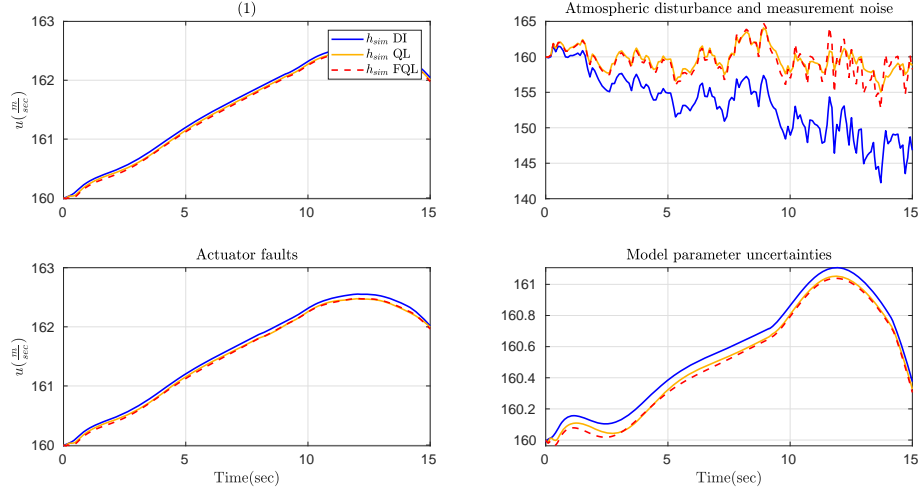


Figure 10: Simulated longitudinal speed results during various scenarios

to its control effort. More precisely about ideal conditions, the altitude tracking errors of QL and FQL are slightly better than DI, unlike their control effort. However, the differences are insignificant. As previously stated in the second scenario, despite DI superiority in pitch and altitude tracking errors, elevator deflection is saturated drastically. In the simulated flight influenced by actuator faults, the FQL controller is the forerunner. In this scenario, QL performance is inferior to that of other controllers, yet all controllers are successful. The final simulated flight includes model parameter uncertainties, and the FQL attitude tracking error is better than the other two. Although altitude tracking error and control effort of DI are superior, the differences are insignificant. Another discussion is around the working area of the proposed FQL controller to prove its robustness. Although the previous simulations were in different flight conditions, they were designed just around one working point. More precisely, they were simulated in initial aircraft longitudinal speed $160 \frac{m}{s}$, and constant aircraft longitudinal aerodynamic and control coefficients. In this part, the performance of both FQL and DI controllers are examined in a wider alteration of aforesaid coefficients and aircraft speed. In this case, the coefficients are varied between $\pm 30\%$, and also the aircraft speed initializes between 150 to $220 \frac{m}{s}$. The FQL findings were satisfactory in comparison with one of the well-

Table 6: Attitude tracking error, altitude tracking error, and control effort of three methods in different flight conditions.

Flight Condition	Control Method	Attitude Tracking Error (deg)	Altitude Tracking Error (m)	Control Effort (deg)
Ideal	Dynamic Inv	0.057	0.662	0.593
	Q-learning	0.047	0.643	0.649
	Fuzzy QL	0.040	0.644	0.669
Noise + Disturbance	Dynamic Inv	2.541	1.477	13.772
	Q-learning	11.178	21.655	1.998
	Fuzzy QL	2.629	2.17	3.954
Actuator Fault	Dynamic Inv	0.075	0.717	0.592
	Q-learning	0.091	0.755	0.624
	Fuzzy QL	0.064	0.708	0.654
Model Uncertainty	Dynamic Inv	0.060	0.903	0.734
	Q-learning	0.056	0.936	0.793
	Fuzzy QL	0.042	0.928	0.812

known robust controllers namely Dynamic Inversion. According to figure 10, the FQL pitch angle tracking error varies between 0.04 to 0.07 degrees during 81 defined initial conditions. Correspondingly, the control effort related to this controller varies between 0.64 to 2.6 degrees. On the other hand, the tracking error of DI computed between 0.05 to 0.07 degrees where the elevator control effort is varied from 0.7 to 2,6 degrees.

7. Conclusion

In this research, auto-landing control of a regional jet aircraft with a novel configuration and specific longitudinal dynamic stability characteristics was addressed using Fuzzy Q-learning. The robustness property of this method was evaluated in several probable scenarios including atmospheric disturbances, sensor measurement noise, actuator faults, and model parameter uncertainties. The simulation results illustrated comparable improvements in contrast to Dynamic Inversion and classic Q-learning controllers. An innovative continuous action generator was proposed in this research to be a connector between optimal Q-tables and RL environments. In order to depict the robustness and working area of the proposed method, the aircraft's longitudinal speed, and coefficients have been altered widely, and the pitch angle tracking error as well as control effort are

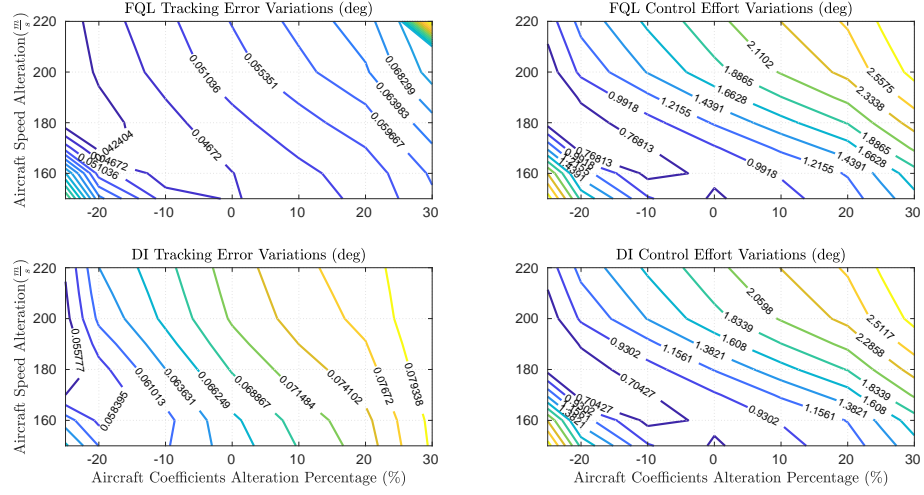


Figure 11: Fuzzy Q-learning and Dynamic Inversion tracking error and control effort examined by alteration of model parameters, and aircraft speeds

reported numerically. Summing up, the competency of the Fuzzy Q-learning method was proved in this problem approaching different flight conditions without being stuck in complicated Artificial Neural Network architectures.

References

- [1] Li Li, Junqiang Bai, and Feng Qu. Multipoint aerodynamic shape optimization of a truss-braced-wing aircraft. *Journal of Aircraft*, pages 1–16, 2022.
- [2] Martin Sohst, José Lobo do Vale, Frederico Afonso, and Afzal Suleman. Optimization and comparison of strut-braced and high aspect ratio wing aircraft configurations including flutter analysis with geometric non-linearities. *Aerospace Science and Technology*, 124:107531, 2022.
- [3] Timothy Chau and David W Zingg. Aerodynamic design optimization of a transonic strut-braced-wing regional aircraft. *Journal of Aircraft*, 59(1):253–271, 2022.
- [4] S. Zavaree, M. Zahmatkesh, K. Eghbali, K. Zahiremani, E. Vaezi, s.A. Madani, A. Kariman, Z. Heidari, A. Mahmoudi, F. Rassouli, et al. Modern regional jet family (chaka: A high- performance, cost-efficient, semi-conventional regional jet family), 2021.
- [5] Nhan T Nguyen and Juntao Xiong. Dynamic aeroelastic flight dynamic modeling of mach 0.745 transonic truss-braced wing. In *AIAA SCITECH 2022 Forum*, page 1325, 2022.
- [6] Arthur Suharev, Vladimir Shestakov, and Konrad Stefański. Analysis of the affecting factors on aircraft takeoff and landing ground path length. 2019.
- [7] Batuhan Eroglu, M. Cagatay Sahin, and Nazim Kemal Ure. Autolanding control system design with deep learning based fault estimation. *Aerospace Science and Technology*, 102:105855, 2020.
- [8] Mihai Lungu. Backstepping and dynamic inversion control techniques for automatic landing of fixed wing unmanned aerial vehicles. *Aerospace Science and Technology*, 120:107261, 2022.
- [9] Shaik Ismail, Abhay A. Pashilkar, Ramakalyan Ayyagari, and Narasimhan Sundararajan. Improved neural-aided sliding mode controller for autolanding under actuator failures and severe winds. *Aerospace Science and Technology*, 33(1):55–64, 2014.
- [10] Zhuang Wang, Hui Li, Haolin Wu, Feng Shen, and Ruixuan Lu. Design of agent training environment for aircraft landing guidance based on deep reinforcement learning. In *2018 11th International Symposium on Computational Intelligence and Design (ISCID)*, volume 02, pages 76–79, 2018.
- [11] Xin Yuan, Yuewen Sun, Yuanda Wang, and Changyin Sun. Deterministic policy gradient with advantage function for fixed wing uav automatic landing. In *2019 Chinese Control Conference (CCC)*, pages 8305–8310, 2019.
- [12] Chi Tang and Ying-Chih Lai. Deep reinforcement learning automatic landing control of fixed-wing aircraft using deep deterministic policy gradient. In *2020 International Conference on Unmanned Aircraft Systems (ICUAS)*, pages 1–9, 2020.
- [13] Fang Liao, Jian Liang Wang, Eng Kee Poh, and Dong Li. Fault-tolerant robust automatic landing control design. *Journal of guidance, control, and dynamics*, 28(5):854–871, 2005.
- [14] A.A. Pashilkar, N. Sundararajan, and P. Saratchandran. A fault-tolerant neural aided controller for aircraft auto-landing. *Aerospace Science and Technology*, 10(1):49–61, 2006.
- [15] George Zogopoulos-Papaliakos, George C Karras, and Kostas J Kyriakopoulos. A fault-tolerant control scheme for fixed-wing uavs with flight envelope awareness. *Journal of Intelligent & Robotic Systems*, 102(2):1–33, 2021.
- [16] Salman Ijaz, Lin Yan, Mirza Tariq Hamayun, and Cun Shi. Active fault tolerant control scheme

- for aircraft with dissimilar redundant actuation system subject to hydraulic failure. *Journal of the Franklin Institute*, 356(3):1302–1332, 2019.
- [17] Kijoon Kim, Seungkeun Kim, Jinyoung Suk, Jongmin Ahn, Nakwan Kim, and Byoung-Soo Kim. Flight test of flying-wing type unmanned aerial vehicle with partial wing-loss. *Proceedings of the Institution of Mechanical Engineers, Part G: Journal of Aerospace Engineering*, 233(5):1611–1628, 2019.
 - [18] Mikkel Eske Nørgaard Sørensen, Søren Hansen, Morten Breivik, and Mogens Blanke. Performance comparison of controllers with fault-dependent control allocation for uavs. *Journal of Intelligent & Robotic Systems*, 87(1):187–207, 2017.
 - [19] Xiaowei Yang, Xixiang Yang, and Xiaolong Deng. Horizontal trajectory control of stratospheric airships in wind field using q-learning algorithm. *Aerospace Science and Technology*, 106:106100, 2020.
 - [20] Zeyi Xi, Di Wu, Wenjun Ni, and Xiaoping Ma. Energy-optimized trajectory planning for solar-powered aircraft in a wind field using reinforcement learning. *IEEE Access*, 10:87715–87732, 2022.
 - [21] Eivind Bøhn, Erlend M Coates, Dirk Reinhardt, and Tor Arne Johansen. Data-efficient deep reinforcement learning for attitude control of fixed-wing uavs: Field experiments. *arXiv preprint arXiv:2111.04153*, 2021.
 - [22] Weijun Hu, Zhiqiang Gao, Jiale Quan, Xianlong Ma, Jingyi Xiong, and Weijie Zhang. Fixed-wing stalled maneuver control technology based on deep reinforcement learning. In *2022 IEEE 5th International Conference on Big Data and Artificial Intelligence (BD AI)*, pages 19–25. IEEE, 2022.
 - [23] David J. Richter, Lance Natonski, Xiaxin Shen, and Ricardo A. Calix. Attitude control for fixed-wing aircraft using q-learning. In Jong-Hoon Kim, Madhusudan Singh, Javed Khan, Uma Shanker Tiwary, Marigankar Sur, and Dhananjay Singh, editors, *Intelligent Human Computer Interaction*, pages 647–658, Cham, 2022. Springer International Publishing.
 - [24] Christopher JCH Watkins and Peter Dayan. Q-learning. *Machine learning*, 8(3):279–292, 1992.
 - [25] P.Y. Glorennec and L. Jouffe. Fuzzy q-learning. In *Proceedings of 6th International Fuzzy Systems Conference*, volume 2, pages 659–662 vol.2, 1997.
 - [26] Arga Dwi Pambudi, Trihastuti Agustinah, and Rusdhianto Effendi. Reinforcement point and fuzzy input design of fuzzy q-learning for mobile robot navigation system. In *2019 International Conference of Artificial Intelligence and Information Technology (ICAIIIT)*, pages 186–191, 2019.
 - [27] Meng Joo Er and Chang Deng. Online tuning of fuzzy inference systems using dynamic fuzzy q-learning. *IEEE Transactions on Systems, Man, and Cybernetics, Part B (Cybernetics)*, 34(3):1478–1489, 2004.
 - [28] Vu Phi Tran, Mohamed A. Mabrok, Sreenatha G. Anavatti, Matthew A. Garratt, and Ian R. Petersen. Robust fuzzy q-learning-based strictly negative imaginary tracking controllers for the uncertain quadrotor systems. *IEEE Transactions on Cybernetics*, pages 1–13, 2022.
 - [29] Mohsen Zahmatkesh, Seyyed Ali Emami, Afshin Banazadeh, and Paolo Castaldi. Robust attitude control of an agile aircraft using improved q-learning. *Actuators*, 11(12), 2022.

- [30] Marcello R Napolitano. *Aircraft Dynamics*. Wiley, 2012.
- [31] PH Zipfel. Modeling and simulation of aerospace vehicle dynamics—third edition, 2014.
- [32] Andrew Wood, Ali Sydney, Peter Chin, Bishal Thapa, and Ryan Ross. Gymfg: A framework with a gym interface for flightgear. *arXiv preprint arXiv:2004.12481*, 2020.
- [33] Jan Roskam. *Airplane flight dynamics and automatic flight controls*. DARcorporation, 1998.
- [34] VA Mil-f. 8785c: Flying qualities of piloted airplanes. *US Air Force*, 5, 1980.
- [35] Walter Frost and Roland L Bowles. Wind shear terms in the equations of aircraft motion. *Journal of Aircraft*, 21(11):866–872, 1984.
- [36] John Anderson. *Aircraft Performance and Design*. WCB/McGraw-Hill, 1 edition, 1999.
- [37] Pradeep R. Ambati and Radhakant Padhi. Robust auto-landing of fixed-wing uavs using neuro-adaptive design. *Control Engineering Practice*, 60:218–232, 2017.
- [38] Ender Çetin. System identification and control of a fixed wing aircraft by using flight data obtained from x-plane flight simulator. Master’s thesis, Middle East Technical University, 2018.
- [39] Richard S Sutton and Andrew G Barto. *Reinforcement learning: An introduction*. MIT press, 2018.